Energy levels and band offsets at interfaces from first-principles: example of asymmetric Hubbard dimer

Jean Goossaert
Under the supervision of Vitaly Gorelov & Matteo Gatti

M2 ICFP, Condensed matter
Laboratory: LSI, Palaiseau
from April 9th to June 28th 2024

Abstract

In this Master's thesis, we explore different many-body approximations applied to the simplest model that can be used to describe interfaces between materials: the asymmetric Hubbard dimer. We start with effective independent-particle schemes, namely Kohn-Sham Density functional theory (KS DFT), which can be performed without approximation here, and the Hartree-Fock approximation (HF), both restricted and unrestricted. Then, the GW approximation is presented and adapted to the model, where G is the one-body Green's function and W the screened Coulomb potential. We explored four different flavours of GW: two different independent-particle Green's functions and two screened potentials, W_0 (approximate) and W (exact). Interestingly, the use of the exact screened potential turned out to give less accurate results than W_0, computed with the Random Phase Approximation (RPA) and a non-interacting Green's function. This work is the first step of a benchmark study of many-body approximations applied for band offset problems in photovoltaic materials.

Contents

1 Introduction

The development of more efficient renewable energy sources is urgent to tackle the environmental crisis. One of the first that come to mind, solar panels, are based on a technology that was developed in the 1950's and is still used today: hetero-junctions of semi-conductors. The idea is very simple, a photon is absorbed by the main semi-conductor, silicon for instance, producing an electron-hole pair that is free to move within the material until it reaches the junction. There, a small shift in the band structure between the two materials is designed such that the electron-hole pair breaks, creating a current. Thus, the efficiency of a photovoltaic material depends - among other things - on the energy level alignment of the two materials at the interface, called the band offset. But behind such a simple mechanism, that we easily interpret within the independent electron picture, lies the incredibly difficult "Many body problem" that makes band structure and bare particles not well-defined when correlations become strong. How then to correctly model this problem, if we want to improve this technology?

Among the different ways used to measure band alignment between two materials, the most common one is photoemission spectroscopy. The idea is the following: light is first shone at a given frequency on the first material alone (typically silicon), removing electrons by photoelectric effect. The kinetic energy of these electrons is then measured, revealing the band structure of the bulk material. Thin layers of the interface material are then deposited on top, and the photoemission measurements are repeated each time. Contrary to the valence bands, the core energies are not too strongly affected during this process, and the measure of their offset allows to deduce the valence band offset. This is called Kraut's method, and it is explained in [1].

On the other hand, from the theoretician's point of view, many strategies are often used to explore beyond the single-particle picture: Kohn-Sham Density Functional Theory (KS DFT), Dynamical Mean Field Theory (DMFT), GW approximations, quantum Monte Carlo methods... Each of these has its own range of validity, which may not be easy to evaluate for real materials. Specific methods have been developed to adapt these many-body frameworks to the band offset problem (see for example [2]). A first problem arises: what methods and approximations to use in order to calculate band offsets in good agreement with the experiments? A second major problem, which may even be more fundamental, is the following. The very definition of band offsets relies on the independent-particle picture, while what experimentalists measure, and theoreticians try to compute, are addition/removal energies, which are fundamentally many-body quantities. Therefore, is it always possible to define a band offset, and how?

The goal of this internship (followed by a PhD) is to benchmark many different ways to evaluate band offsets in real systems, in such a way that experimentalists and theoreticians can rigorously compare their results. We start simple in this thesis by exploring a toy model: the Hubbard dimer. The great advantage of this model, which is the simplest hetero-junction one can think of, is that it is exactly solvable, allowing for comparison between the approximate many-body energies to the exact ones.

In the first section, the theoretical model is presented as well as its exact solutions. Then, an exact KS DFT study is performed, followed by the HF approximation, constituting the two main independent-particle schemes. After that, the GW approximation is presented and applied to the model, using first the approximate W_0 screened interaction and then the exact one. Finally, the link with real materials is made through a discussion of band offsets for the Hubbard dimer.

2 The Hubbard dimer model

2.1 The model

The simplest model describing the physics near the junction between two different materials is the asymmetric Hubbard dimer, in which each material is represented by a single site that can host at most two electrons, due to the Pauli principle. A given electron will then have a kinetic energy given by a probability amplitude t to hop from one site to the other, as well as an on-site potential energy v_i, different for the two sites. Finally, we consider only local and spin-dependent electron-electron repulsion of amplitude U, taking into account simultaneously Coulomb force and Pauli's exclusion principle. The resulting Hamiltonian reads:

$$H = -t \sum_{\sigma} (\hat{c}^{\dagger}_{1\sigma} \hat{c}_{2\sigma} + h.c) + U \sum_{i} \hat{n}_{i\uparrow} \hat{n}_{i\downarrow} + \sum_{i} v_i \hat{n}_i \, . \tag{2.1}$$

We choose the convention $2t = 1$ and $v_1 + v_2 = 0$, leaving only two free parameters, $\Delta v = v_2 - v_1$ and U. We will work in the canonical ensemble, where the number N of electrons is fixed. The symmetric limit $\Delta v \to 0$ as well as the asymmetric one for $N = 1$ have been studied in the group, respectively in [3] and [4]. In this project, I focused on the half-filled ($N = 2$) asymmetric case. In the following, we call occupation numbers the quantities $n_i = \langle \hat{n}_i \rangle$ ($i = 1, 2$), and occupation difference $\Delta n = n_1 - n_2$.

2.2 Exact eigenenergies

For $N = 1$ and $N = 3$, the Hilbert space is of dimension 4, and H is easy to diagonalise. For $N = 2$, if we impose that the total spin S_z is zero[1], we also have a four-dimensional Hamiltonian to diagonalise, and more sophisticated solutions appear. In Tab. 1, the eigenenergies are written for these three cases, while the eigenstates are written in appendix A.

$N = 1$	$N = 2$	$N = 3$
$E_{-}^{N=1} = -\frac{1}{2}\sqrt{4t^2 + \Delta v^2}$	$E_{\lambda}^{N=2} = \frac{2}{3}\left[U - r\cos(\theta + \phi_{\lambda})\right]$	$E_{-}^{N=3} = -\frac{1}{2}\sqrt{4t^2 + \Delta v^2} + U$
$E_{+}^{N=1} = \frac{1}{2}\sqrt{4t^2 + \Delta v^2}$	$E_{2}^{N=2} = 0$	$E_{+}^{N=3} = \frac{1}{2}\sqrt{4t^2 + \Delta v^2} + U$

Table 1: Exact eigenenergies of the Hubbard dimer model for $N = 1, 2, 3$, where $z^2 = 9\Delta v^2 - U^2 - 19t^2$, $r^2 = 3\Delta v^2 + U^2 + 12t^2$ and $\cos(3\theta) = \frac{z^2 U}{r^3}$

2.3 Exact one-body Green's function

In principle, all the information about a given many-body system is contained in the many-body wavefunction, or equivalently in the many-body Green's function, whose equation of motion is equivalent to the full Schrödinger equation. However, such a quantity contains too much information, and most observables can be computed from the retarded one-body Green's function

[1] We are indeed not interested in ferromagnetic systems

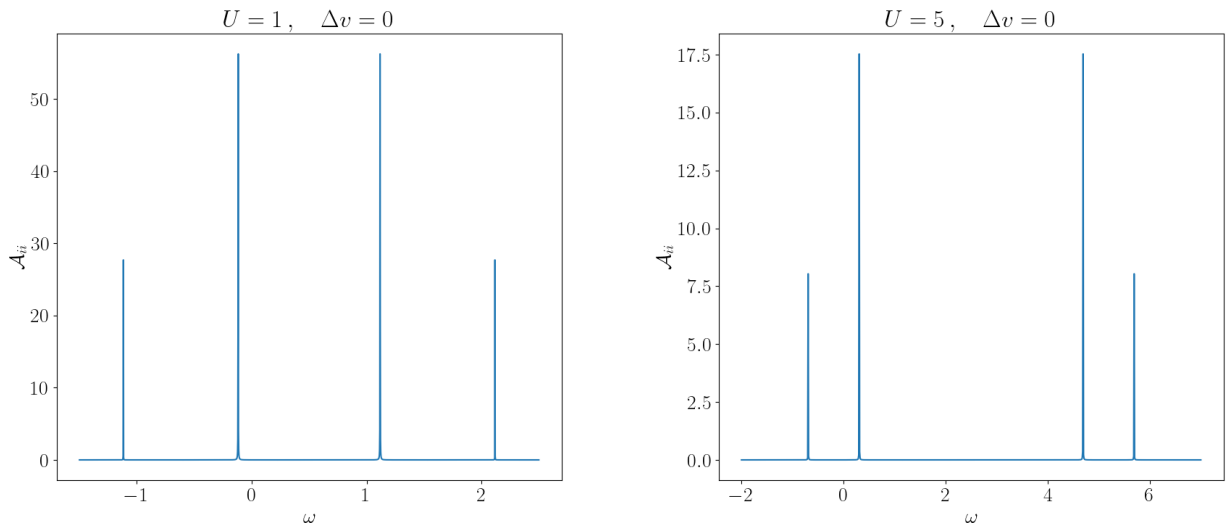

Figure 1: Exact spectral function $\mathcal{A}(\omega)$ for $U = 1$ and $U = 5$, in the symmetric case $\Delta v = 0$.

(1-GF), which is defined by:

$$G_{ij\sigma}(\omega) = -i \int_{-\infty}^{+\infty} \mathrm{d}t e^{i\omega t} \left\langle \hat{T} \left[\hat{c}_{i,\sigma}(t) \hat{c}^{\dagger}_{j,\sigma} \right] \right\rangle , \tag{2.2}$$

where the expectation value is taken at the ground state[2] and $\hat{T}$ is the time-ordering operator, ensuring causality. The 1-GF has a more physical expression in the Lehmann representation (Eq. 2.3), where we clearly see that its poles are the energies needed to add or remove one electron to or from the system. These are precisely the energies that are measured in photoemission experiments, and we will call them energy levels in the following.

$$\begin{aligned} G^{N=2}_{ij\sigma}(\omega) \;=\; & \sum_{n=1}^{4} \frac{\langle \lambda = 1 | \, c_{i\sigma} \left| \psi^{N=3}_n \right\rangle \left\langle \psi^{N=3}_n \right| c^{\dagger}_{j\sigma} \, | \lambda = 1 \rangle}{\omega + i0^+ - (E^{N=3}_n - E_1)} \\ & + \sum_{n=1}^{4} \frac{\langle \lambda = 1 | \, c^{\dagger}_{i\sigma} \left| \psi^{N=1}_n \right\rangle \left\langle \psi^{N=1}_n \right| c_{j\sigma} \, | \lambda = 1 \rangle}{\omega - i0^+ - (E_1 - E^{N=1}_n)} \,, \end{aligned} \tag{2.3}$$

where $|\lambda = 1\rangle$ is the ground state for $N = 2$, given by Eq. A.6. Thanks to the Lehmann representation and the exact eigenstates, we can compute exactly each component $G^{N=2}_{ij\sigma}(\omega)$ analytically. From these we can compute the spectral function, which is an extension of the notion of density of states in many-body physics:

$$\mathcal{A}_{ij\sigma}(\omega) = -\frac{1}{\pi} \mathfrak{Im}\, G_{ij\sigma}(\omega) \qquad \text{and} \qquad \mathcal{A}(\omega) = \sum_{i,\sigma} \mathcal{A}_{ii\sigma}(\omega) \,. \tag{2.4}$$

The exact spectral function is plotted for $\Delta v = 0$ and two different values of U in Fig.1. The

[2]The same notation can be used to define the 1-GF at non-zero temperature. In this thesis, we will always consider $T = 0$.

two main peaks are called quasi-particle peaks and their position correspond to the energies of adding / removing one electron. The two lower peaks are called satellites and are excitations due to electron-electron interactions. We can note that, as expected in the symmetric case $\Delta v = 0$, the spectral function is symmetric around $\Delta v = \frac{U}{2}$.

Finally, the 1-GF is solution of the equation of motion Eq. B.1, in which the second term defines the self-energy Σ, an object that effectively takes into account the electronic correlations. Σ, G and G_0, the non-interacting 1-GF (which is the 1-GF for $U = 0$) are linked by Dyson's equation (written here in an arbitrary basis):

$$G^{-1} = G_0^{-1} + \Sigma \tag{2.5}$$

3 Exact Kohn-Sham study

Kohn-Sham density functional theory (KS DFT) is a very common tool which is widely used to quickly compute the band structure of materials. It is said to be an *ab initio* method since it starts with the real fundamental Hamiltonian of the system instead of relying on models (such as the Hubbard one). DFT is based on the Hohenberg–Kohn [5] theorems which state that all observables can be expressed as a functional of the electronic ground state density $n(\mathbf{r})$. The genius idea by Kohn and Sham [6], that makes DFT a very useful framework, is then to substitute the real system by a non-interacting one that provides the same density. In that sense, the KS scheme is exact.

In our discrete model, the density is no longer a function but a set of two numbers n_1 and $n_2 = N - n_1$. Thus, we should rather work with Site-Occupation Function Theory (SOFT), introduced in [7] and applied to the Hubbard dimer in [8]. The main quantities of interest are summarised in Tab. 2, for both the real and the fictitious systems.

	Real system	Fictitious KS system
Universal function(al)	$F(n_1) = E(n_1) - V(n_1)$	$F(n_1) = T_s(n_1) + U_H(n_1) + E_x(n_1) + E_c(n_1)$
External potential	Δv	Δv_s
Electronic density	Δn	Δn
Electron interactions	Yes	No

Table 2: Summary of the differences between the real and the fictitious systems

The bridge between the two systems is given by the universal functional F, which is defined by everything in the energy that does not depend on the specific material (i.e the kinetic and correlation energies of the electrons). In our case, it can be computed exactly since we know the ground state energy E_1 and the external potential energy:

$$V(n_1) = \left\langle \hat{V} \right\rangle = v_1 n_1 + v_2 n_2 = -\frac{\Delta v}{2} n_1 + \frac{\Delta v}{2} n_2 = -\frac{\Delta n \Delta v}{2} \tag{3.1}$$

And thus:

$$F(n_1) = E_1(n_1) + \frac{\Delta n \Delta v}{2} \qquad \text{with} \qquad \Delta n = 2n_1 - N \tag{3.2}$$

Knowing exactly F is only possible because we already solved the problem exactly, and it enables us to compute the correlation energy $E_c = F - T_s - U_H - E_x$. In real systems, F is unknown, and E_c has to be approximated (for instance with the local density approximation).

Since the fictitious system is non interacting, its Hamiltonian is separable into two one-particle Hamiltonians that are the same as the real one for $N = 1$ (see Eq. A.1), but with effective on-site potentials v_s^1 and v_s^2. The corresponding Kohn-Sham (KS) eigenenergies are thus:

$$\boxed{\epsilon_\pm^{\mathrm{KS}} = \pm\frac{1}{2}\sqrt{4t^2 + \Delta v_s^2} + \bar{v}_s} \tag{3.3}$$

where, thanks to the $N = 1$ useful formula A.4, we find by inverting the KS equation that Δv_s is given by[3]:

$$\Delta v_s = \frac{2t\Delta n}{\sqrt{4 - \Delta n^2}} \tag{3.4}$$

and $\bar{v}_s = \frac{U}{2} + \bar{v}_c$, with $v_c^i = v_c^1 + v_c^2$. However, KS DFT only fixes v_c^i up to a constant. A way to fix that constant is to remark that $v_c^i = \frac{\mathrm{d}E_c}{\mathrm{d}n_i}$ and to use a chain rule:

$$\bar{v}_c = \left.\frac{\partial E_c}{\partial N}\right|_{\Delta n, N=2^-} \tag{3.5}$$

The derivative of E_c with respect to N is known to be discontinuous at integer values of N, and we decide here to evaluate it for $N = 2^-$. This poses a new problem: we need to define our functionals for fractional number of particles (i.e to work in the grand canonical ensemble). As suggested in [8], the ground state energy and the occupation difference for fractional $\mathcal{N} = 1 + \omega$ are:

$$\begin{cases} E_1^{\mathcal{N}} = \omega E_1^{N=2} + (1-\omega)E_1^{N=1} \\ \Delta n^{\mathcal{N}} = \omega \Delta n^{N=2} + (1-\omega)\Delta n^{N=1} \end{cases} \tag{3.6}$$

Numerically inverting the second equation in 3.6 allows us to find $\Delta v^{\mathcal{N}}(\Delta n)$ for fixed $\mathcal{N}$ and Δn, which combined with the second equation in 3.6 allows us to compute $E_c(\mathcal{N}, \Delta n)$ and thus $\bar{v}_s$.

The final KS energies $\epsilon_\pm^{KS}$ are plotted in Fig. 2 on top of the energy levels $E_{\mathrm{GS}}^{N+1} - E_{\mathrm{GS}}^N$, corresponding to the change of energy when adding or removing one electron to the $N = 2$ system in the ground state (GS). These are the energies that we indeed measure experimentally, and are the poles of the one-body Green's function, as discussed in Sec. 2.3. According to Koopmans' theorem for KS DFT, we are supposed to find that the lower KS energy ϵ_-^{KS} (called HOMO in the chemistry community, for *Highest Occupied Molecular Orbital*) is equal to the opposite of the ionisation energy $I = E_-^{N=1} - E_0^{N=2}$, i.e the energy cost of removing one electron. This is indeed verified for $U = 1$ and $U = 5$ in Fig. 2. The upper KS energy ϵ_+^{KS} (called LUMO, for *Lowest*

[3]Actually, inverting A.4 gives two solutions, one of which is negative and the other positive. The negative one can though be discarded since in the ground state, when $\Delta n = n_1 - n_2 > 0$, more electrons lie on site 1, thus we must have $v_1 < v_2$, i.e $\Delta v > 0$.

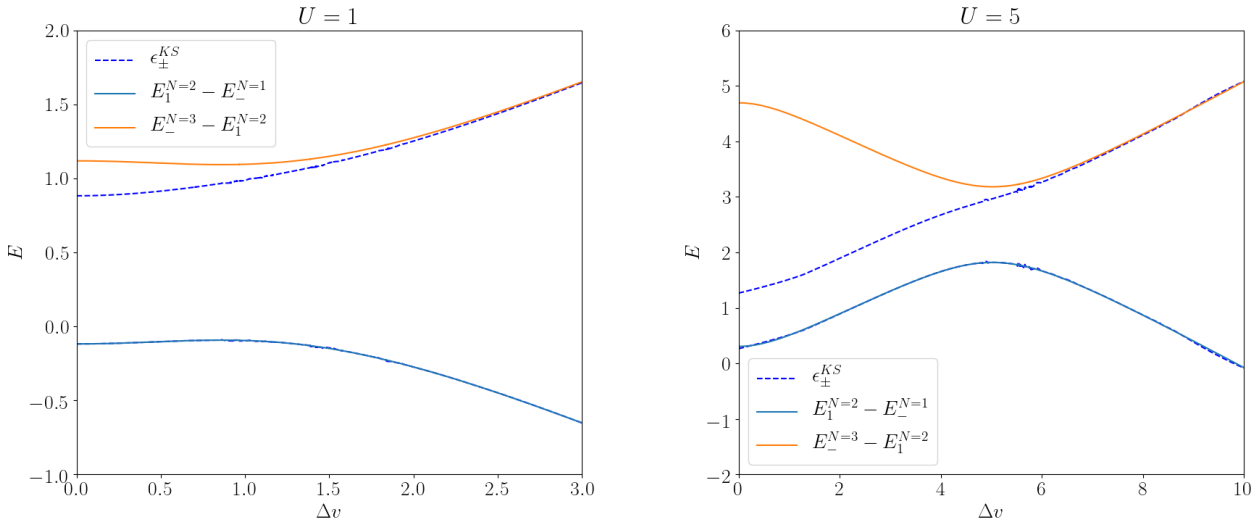

Figure 2: Comparison between the exact energy levels and the HOMO and LUMO KS solutions, for $U = 1$ and $U = 5$

Unoccupied Molecular Orbital) is not supposed to have a physical meaning, but it matches well the energy for adding one electron for small U and/or large Δv. It is interesting to note that, despite being exact, the KS scheme does not give exact energy levels (it is indeed only designed to give the exact GS occupation numbers). Only in the low correlation limit are these eigenenergies good approximations for the measured energy levels.

In practice, approximations have to be found for computing E_c, such as the Local Density Approximation (LDA), leading to less accurate energies.

4 A mean-field approach: the Hartree-Fock approximation

In the previous section, we explored the exact KS scheme, which was exact in the sense that the KS auxiliary system gives the exact ground state occupation number. A fundamentally different approach is to start from the Hubbard Hamiltonian 2.1 and approximate it. A natural approximation to obtain a separable Hamiltonian that takes into account some interactions in an effective way is to model electronic interactions as a mean field. We expect this approximation to fail in the large U limit, where a mean-field approach does not apply anymore.

There are several ways to derive the Hartree-Fock (HF) approximation. One natural way is to start from the Hamiltonian and re-write the interaction term as:

$$n_{i\uparrow}n_{i\downarrow} = \overline{n}_{i\uparrow}n_{i\downarrow} + \overline{n}_{i\downarrow}n_{i\uparrow} - \overline{n}_{i\uparrow}\overline{n}_{i\downarrow} + \cancel{(n_{i\uparrow} - \overline{n}_{i\uparrow})(n_{i\downarrow} - \overline{n}_{i\downarrow})} \tag{4.1}$$

which gives rise to a single-electron Hamiltonian feeling an effective potential $v_{i\sigma}^{\text{eff}}$:

$$H^{\text{H}} = \sum_{i,\sigma} \left[-t(c_{i\sigma}^{\dagger}c_{i+1,\sigma} + hc) + v_{i\sigma}^{\text{H}} \right] \qquad \text{with} \qquad v_{i\sigma}^{\text{eff}} = v_i + Un_{i\overline{\sigma}} \tag{4.2}$$

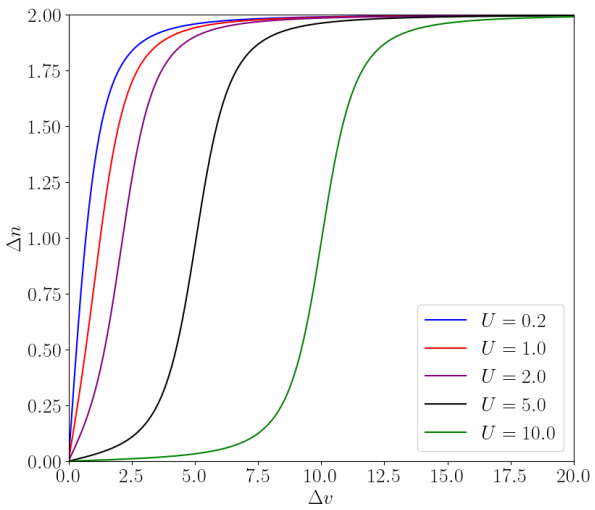

(a) Exact solution

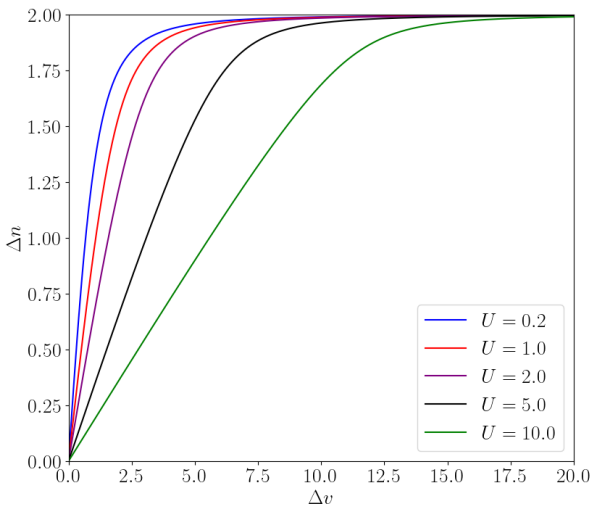

(b) Restricted HF formula solved self-consistently

Figure 3: Δn with respect to Δv both in the exact scheme and the RHF approximation Eq. 4.7

where "H" stands for Hartree. This Hamiltonian is still hard to solve, since it now depends on $n_{i\uparrow}$ and $n_{i\downarrow}$. We can first make the approximation that the local magnetisation $m_i = n_{i\uparrow} - n_{i\downarrow}$ is zero, i.e that $n_{i\uparrow} = n_{i\downarrow} = \frac{n_i}{2}$. This is a paramagnetic approximation (since it does not allow ferro/anti-ferromagnetic solutions), and is called restricted Hartree-Fock (RHF).

4.1 Restricted Hartree-Fock

In this case the single-electron Hamiltonian can be written in the basis $(|\uparrow, 0\rangle, |\downarrow, 0\rangle, |0, \uparrow\rangle, |0, \downarrow\rangle)$ as:

$$h^{\mathrm{RH}} = \begin{pmatrix} v_1 + \frac{Un_1}{2} & 0 & -t & 0 \\ 0 & v_1 + \frac{Un_1}{2} & 0 & -t \\ -t & 0 & v_2 + \frac{Un_2}{2} & 0 \\ 0 & -t & 0 & v_2 + \frac{Un_2}{2} \end{pmatrix} \tag{4.3}$$

which looks very similar to $H^{N=1}$ (see Eq. A.1) with effective onsite potentials $v_i^{\mathrm{eff}} = v_i + \frac{Un_i}{2}$. Diagonalising this Hamiltonian gives two degenerate eigenvalues[4]:

$$\epsilon_{\pm}^{\mathrm{RH}} = \frac{v_1^{\mathrm{eff}} + v_2^{\mathrm{eff}}}{2} \pm \frac{1}{2}\sqrt{4t^2 + (\Delta v^{\mathrm{eff}})^2} \implies \boxed{\epsilon_{\pm}^{\mathrm{RH}} = \frac{U}{2} \pm \frac{1}{2}\sqrt{4t^2 + (\Delta v^{\mathrm{eff}})^2}} \tag{4.4}$$

The difficulty here is that the energy still depends on the site occupation Δn, which we have to calculate for a given Δv. Since the system is separable within the HF approximation, the ground state is a Slater determinant $|\Phi\rangle$ composed of twice the ground state $|-\rangle$ of h^{RH}. Thus, we simply have:

$$n_i = \langle\Phi|\, \hat{n}_i \,|\Phi\rangle = 2\,\langle -|\, \hat{n}_i \,|-\rangle \tag{4.5}$$

[4]We call these energies $\epsilon_{\pm}^{\mathrm{RH}}$, for "Restricted Hartree", instead of RHF. Indeed, a Fock term is to be added when calculating total energies, which we are not of our interest. However, we will continue referring to this approximation as Hartree-Fock in the following.

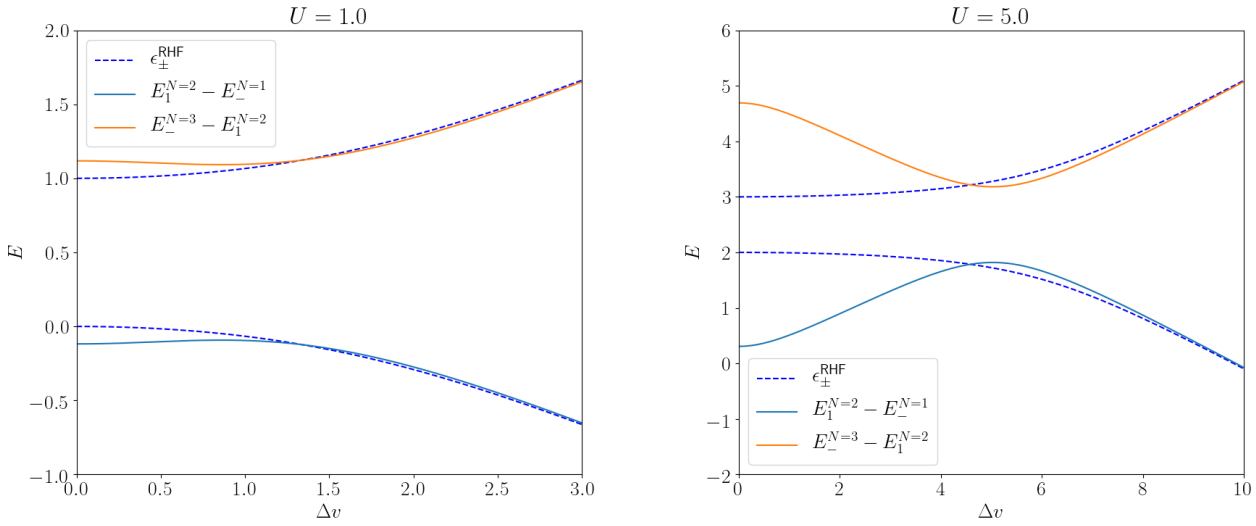

Figure 4: Comparison between the exact energy levels and the HOMO and LUMO RHF solutions, for $U = 1$ and $U = 5$

With, as for the Hubbard dimer with $N = 1$, the single-electron ground state being:

$$|-\rangle = \cos\rho\,|\uparrow,0\rangle + \sin\rho\,|0,\uparrow\rangle \implies \begin{cases} n_1 = 2\cos^2\rho \\ n_2 = 2\sin^2\rho \end{cases} \tag{4.6}$$

Which gives:

$$\Delta n = 2\cos^2\rho - 2\sin^2\rho = 2\,\frac{1-\tan^2\rho}{1+\tan^2\rho} \qquad \text{with} \qquad \tan\rho = \sqrt{1+\left(\frac{\Delta v^{\text{eff}}}{2t}\right)^2} - \frac{\Delta v^{\text{eff}}}{2t} \tag{4.7}$$

This last equation is self-consistent since $\Delta v^{\text{eff}} = \Delta v - \frac{U\Delta n}{2}$. We can solve it self-consistently and we end up with Fig. 3b, that differs significantly from the exact solution (see Fig. 3a) at large U and small Δv, i.e in the high-correlation regime.

Finally, as for the exact KS treatment, we can look at the energy levels $E_1^{N=2} - E_+^{N=1}$ and $E_+^{N=3} - E_1^{N=2}$, and compare them to the restricted Hartree eigenvalues found in Eq. 4.4. Indeed, according to Koopman's theorem, the Hartree-Fock eigenvalues are addition/removal energies. The resulting plots are shown in Fig. 4. As for exact KS, $\epsilon_\pm^{\text{RH}}$ tend to the exact energy levels at low U and large Δv, but fail otherwise. Even though the RHF solutions look very different than the KS ones (the first being symmetric while the second are very asymmetric), the fundamental gap $\epsilon_+ - \epsilon_-$ are about the same, and independent of U, which is remarkable.

A very useful interpretation of the HF solutions is given by Koopman's theorem, according to which the HF eigenenergies (Eq. 4.4) can be physically interpreted as energy levels. This will be used in Sec. 7.

4.2 Unrestricted Hartree-Fock

In order to improve the previous results, we can relax the constraint $m_i = 0$, allowing a local magnetization. According to [8], the ferromagnetic solution ($M = m_1 + m_2 = 2$) is always less

favourable than the antiferromagnetic one ($M = 0$), and we will thus focus on the last one. We can notice that the Hamiltonian 4.2 is block-diagonal in spin-subspace:

$$H^{\mathrm{H}} = \sum_{\sigma} h^{\mathrm{H}}_{\sigma} \qquad \text{with} \qquad h^{\mathrm{H}}_{\sigma} = \begin{pmatrix} v^{\mathrm{eff}}_{1,\sigma} & -1 \\ -t & v^{\mathrm{eff}}_{2,\sigma} \end{pmatrix} \tag{4.8}$$

in the one-electron basis $(|1,\sigma\rangle, |2,\sigma\rangle)$. This Hamiltonian is easy to diagonalise, and we find four eigenenergies, that are a generalisation of Eq. 4.4:

$$\epsilon^{\mathrm{UH}}_{\sigma,\pm} = \frac{v^{\mathrm{eff}}_{1,\sigma} + v^{\mathrm{eff}}_{2,\sigma}}{2} \pm \frac{1}{2}\sqrt{4t^2 + (\Delta v^{\mathrm{eff}}_{\sigma})^2} \tag{4.9}$$

that we can re-write in terms of N, Δn and $\Delta m = m_1 - m_2$:

$$\boxed{\epsilon^{\mathrm{UH}}_{\sigma,\pm} = \frac{U}{4}N \pm \frac{1}{2}\sqrt{4t^2 + (\Delta v^{\mathrm{eff}}_{\sigma})^2}} \qquad \text{with} \qquad \Delta v^{\mathrm{eff}}_{\sigma} = \Delta v - \frac{U}{2}(\Delta n - \sigma \Delta m) \tag{4.10}$$

In order to compute these energies, we need to know Δn and Δm for each value of Δv and U. Generalising Eq. A.4, and extending it also to the magnetisation, we get:

$$\Delta n = \sum_{\sigma} \frac{\Delta v^{\mathrm{eff}}_{\sigma}}{\sqrt{4t^2 + (\Delta v^{\mathrm{eff}}_{\sigma})^2}} \qquad \Delta m = \sum_{\sigma} \sigma \frac{\Delta v^{\mathrm{eff}}_{\sigma}}{\sqrt{4t^2 + (\Delta v^{\mathrm{eff}}_{\sigma})^2}} \tag{4.11}$$

These equations are self-consistent, and we have to solve them numerically, simultaneously for Δn and Δm. We proceed by first computing the exact expression of $\Delta n(\Delta v, U)$, and use this value as an initial guess of Δn. For the initial value of Δm, we choose 2, since we want to prioritise the anti-ferromagnetic solution when it exists (we could have chosen -2 as well, the energy would have been the same). We then iterate Equations 4.11 until convergence. We get Fig. 5, which shows the existence of two phases for each U: an antiferromagnetic one for $\Delta v < \Delta v_c(U)$, for which $\Delta m \neq 0$ (spontaneous breaking of symmetry), and a paramagnetic one for $\Delta v > \Delta v_c(U)$, and for which we recover our previous RHF analysis. This phase transition can be seen as a discontinuity in the derivative of Δn.

Finally, as for exact KS and RHF, we plotted in Fig. 6 the HOMO and LUMO energy levels for UHF compared to the exact energy levels. We clearly see that the corrections at $\Delta v < \Delta v_c$ improve significantly the results at $U = 5$, compared to the RHF solution.

We can interpret the relative success of the paramagnetic and anti-ferromagnetic solutions as follows. At large Δv, the two sites are far apart and the two electrons tend to localise on the same site, despite the Coulomb repulsion U. The Pauli principle ensures that the two electrons have opposite spins, and thus $m_1 = m_2 = 0$, i.e $\Delta m = 0$: this explains the paramagnetic phase. On the contrary, at small Δv, the electrons delocalise to form a triplet of opposite spins. Then, $m_1 = -m_2$ and thus $\Delta m = \pm 1$, which explains the anti-ferromagnetic phase.

5 Beyond Hartree-Fock: the G_0W_0 approximation

Another way to think of the HF approximation is the following. The self-energy (defined by Eq. B.2 or equivalently by Eq. 2.5) is written in this approximation as a Hartree term, describing

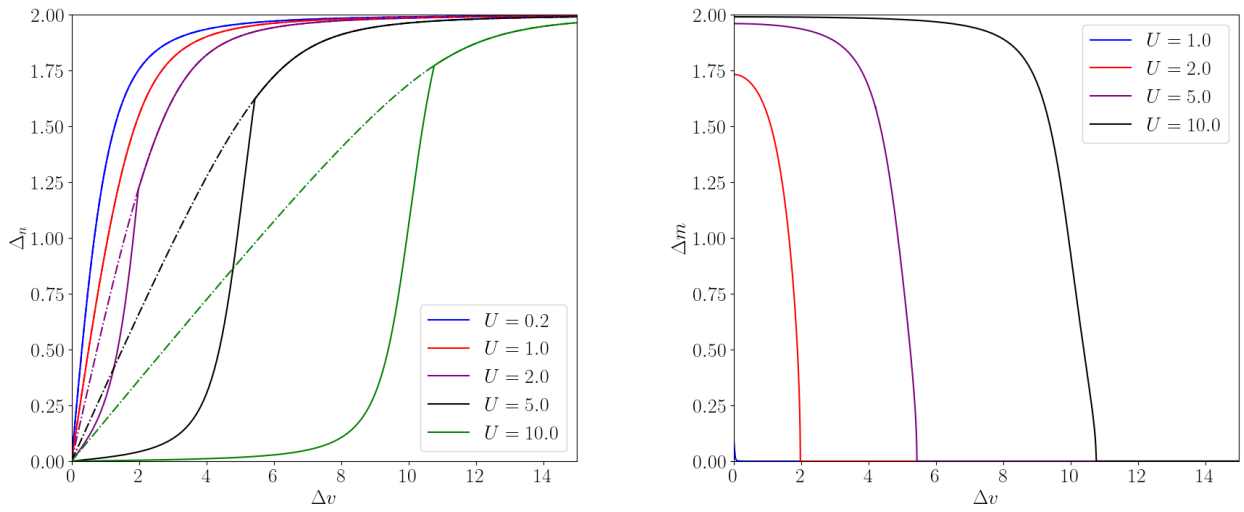

Figure 5: Δn and Δm self-consistently calculated from Eq. 4.11, within the unrestricted antiferromagnetic HF approximation (solid line). The RHF calculation of Δn is also plotted in dashed-dotted lines

naively the interaction of one electron with its environment, and a Fock term that corrects the self-interaction contained in Hartree. We can show that the Fock (or exchange) term reads $\Sigma_x = iGv_{\mathcal{C}}$, where $v_{\mathcal{C}}$ is the Coulomb potential.

This point of view allows for a natural generalisation of the HF approximation, by replacing the Coulomb potential $v_{\mathcal{C}}$ in the Fock term by a dynamically screened Coulomb potential W. Indeed, we know that interacting electrons tend to screen themselves, hugely reducing the potential felt by each individual electron.

5.1 The G_0W_0 approximation

More formally, we show in Appendix B that this dynamically screened HF approximation amounts to take Hedin's equation (Eq. B.5, B.6, B.7, B.8 and 2.5) at first order in W, giving rise to the so-called GW approximation. In particular, we only take into account the first term of $\tilde{\Gamma}$ in Eq. B.6:

$$\tilde{\Gamma}(1,2;3) = \delta(1,2)\delta(1,3)^5 \tag{5.1}$$

Thus, according to Eq. B.5, the self-energy becomes:

$$\boxed{\Sigma^{GW}(1,2) = iG(1,2)W^{\mathrm{RPA}}(2,1^+)} \tag{5.2}$$

where $\tilde{\chi} = \chi_0 = -iGG$ and W are respectively the polarisability and the screened Coulomb potential within the Random Phase Approximation (RPA). We can approximate further and take a non-interacting Green's function G_0 everywhere instead of G, giving rise to the so-called G_0W_0 approximation, that we will explore in the following. Doing so, we avoid the self-consistency of Eq. 5.2. G_0 can either be defined as the 1-GF taken for $U = 0$, or alternatively the 1-GF of an

[5] As explained in Appendix B, a number denotes a set of coordinates: $(1^+) = (\mathbf{r_1}, t_1^+, \sigma_1)$.

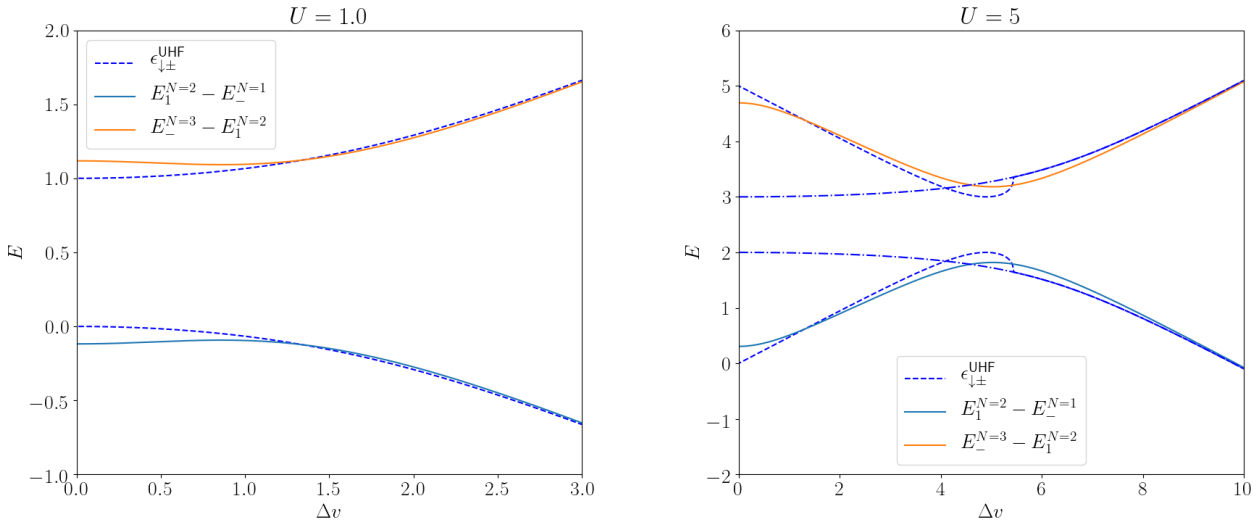

Figure 6: Comparison between the exact energy levels and the HOMO and LUMO UHF solutions, for $U = 1$ and $U = 5$. The RHF calculation is also plotted in dashed-dotted lines for $U = 5$ (for $U = 1$ RHF and UHF are indistinguishable)

auxiliary non-interacting system, such as KS or HF. We expect the second two options to be closer to the exact G, and we will use both of them in our study. Moreover, it will be interesting to compare the results for each choice of G_0.

5.2 G_0W_0 in the case of the asymmetric Hubbard dimer at half-filling

We now want to implement this approximation in our model, where the real-space coordinates will be replaced by sites 1 and 2. In frequency space, the self-energy, the screened Coulomb potential and the irreducible polarisability become:

$$\Sigma_{ij\sigma}(\omega) = i \int \frac{\mathrm{d}\omega'}{2\pi} G^0_{ij\sigma}(\omega + \omega') W^0_{ji}(\omega') e^{i\omega' 0^+} \tag{5.3a}$$

$$W^0_{ij}(\omega) = U\delta_{ij} + U \sum_{k,\sigma,\sigma'} \tilde{\chi}_{ik,\sigma\sigma'}(\omega) W^0_{kj}(\omega) \tag{5.3b}$$

$$\tilde{\chi}_{ij\sigma\sigma'}(\omega) = -i \int \frac{\mathrm{d}\omega}{2\pi} G^0_{ij\sigma}(\omega + \omega') G^0_{ji\sigma'}(\omega') \tag{5.3c}$$

We can thus compute analytically each component $\Sigma_{ij\sigma}(\omega)$ for every choice of G_0.

5.3 Practical implementation

The KS Green's function is a non-interacting one, and thus in the bonding / anti-bonding basis, which is the one-particle eigenstate basis (see Eq. A.2), it reads:

$$G^{\mathrm{KS}}_{\pm\sigma}(\omega) = \langle \pm\sigma | \, \hat{G}^{\mathrm{KS}}(\omega) \, | \pm\sigma \rangle = \frac{1}{\omega - \epsilon^{\mathrm{KS}}_{\pm,\sigma} \pm i0^+} \tag{5.4}$$

which is spin-independent since the KS eigenvalues are. The Green's function in the site basis is thus given by the change of basis:

$$G^{\mathrm{KS}}_{ij,\sigma} = \langle i\sigma |\, \hat{G}^{\mathrm{KS}}(\omega)\, | j\sigma \rangle = \sum_{\pm} \langle i\sigma | \pm\sigma \rangle\, G^{\mathrm{KS}}_{\pm\sigma}(\omega)\, \langle \pm\sigma | j\sigma \rangle = \sum_{\pm} \frac{\phi_{\pm\sigma,i}\phi^{*}_{\pm\sigma,j}}{\omega - \epsilon^{\mathrm{KS}}_{\pm,\sigma} \pm i0^{+}} \tag{5.5}$$

where $\phi_{\pm\sigma,i} = \langle i\sigma|\pm\sigma\rangle$ is given by:

$$\begin{aligned} \phi_{-\sigma,1} &= \cos\rho^{\mathrm{KS}} & \phi_{-\sigma,2} &= \sin\rho^{\mathrm{KS}} \\ \phi_{+\sigma,1} &= \sin\rho^{\mathrm{KS}} & \phi_{+\sigma,2} &= -\cos\rho^{\mathrm{KS}} \end{aligned} \tag{5.6}$$

and ρ^{KS} is defined by Eq. A.3, replacing Δv by Δv_s. The integral expression of $\tilde{\chi}$ (Eq. 5.3c) can now be performed analytically, using the residue theorem:

$$\tilde{\chi}_{ij} = \frac{\tilde{\chi}^{0}_{ij}}{\omega - (\epsilon^{\mathrm{KS}}_{+} - \epsilon^{\mathrm{KS}}_{-}) + i0^{+}} - \frac{\tilde{\chi}^{0}_{ij}}{\omega - (\epsilon^{\mathrm{KS}}_{-} - \epsilon^{\mathrm{KS}}_{+}) - i0^{+}} \tag{5.7}$$

with

$$\tilde{\chi}^{0}_{ij} = 2(-1)^{i-j}\cos^{2}(\rho^{\mathrm{KS}})\sin^{2}(\rho^{\mathrm{KS}}) \tag{5.8}$$

The next step is to compute W_0, which depends self-consistently on W_0 and $\tilde{\chi}$, according to Eq. 5.3b. W_0 is spin-independent, and since $\tilde{\chi}_{11} = \tilde{\chi}_{22} = -\tilde{\chi}_{12} = -\tilde{\chi}_{21}$, it is easy to find that:

$$W^{0}_{ij}(\omega) = U\delta_{ij} + (-1)^{i-j}\frac{tU^{2}}{l\sqrt{1+D^{2}}}\left[\frac{1}{\omega - l + i0^{+}} - \frac{1}{\omega + l - i0^{+}}\right] \tag{5.9}$$

where

$$D = \frac{\Delta v_s}{2t} \qquad \text{and} \qquad l = \sqrt{4t^{2}(1+D^{2}) + \frac{4tU}{\sqrt{1+D^{2}}}} \tag{5.10}$$

Finally, the self-energy is given by the integral 5.3a that, once again, we can perform analytically using the residue theorem:

$$\Sigma^{G_0W_0}_{ij}(\omega) = -\frac{Un_i}{2}\delta_{ij} + \frac{tU^{2}}{l\sqrt{1+D^{2}}}\left[(-1)^{i-j}\frac{|\phi_{-\sigma,i}\phi_{-\sigma,j}|}{\omega - (\epsilon^{\mathrm{KS}}_{-} - l) - i0^{+}} + \frac{|\phi_{+\sigma,i}\phi_{+\sigma,j}|}{\omega - (\epsilon^{\mathrm{KS}}_{+} + l) + i0^{+}}\right] \tag{5.11}$$

where the first term is simply the Hartree term. In this simple form, we directly see that the self energy in this approximation has two poles.

5.4 G_0W_0 energy corrections to exact Kohn-Sham

In order to find the energy levels within the G_0W_0 approximation, we have to solve the Dyson equation satisfied by the G_0W_0 Green's function:

$$(G^{G_0W_0})^{-1} = (G^{\mathrm{KS}}_{0})^{-1} - (\Sigma^{G_0W_0} - V^{\mathrm{KS}}_{xc}) \tag{5.12}$$

and then to find the poles of the associated spectral function, given by:

$$\mathcal{A}^{G_0W_0}(\omega) = -\frac{1}{\pi}\sum_i \mathfrak{Im}\, G_{ii}^{G_0W_0}(\omega) \tag{5.13}$$

In Fig. 7, this G_0W_0 spectral function as well as the exact one (see Sec. 2.3) are plotted in a short range of frequencies around the HOMO and LUMO levels, for $\Delta v = 0$. Finding these two poles numerically from Fig. 7 for many values of Δv is however tedious, and a simpler (approximate) way is to use perturbation theory.

In the end, we are interested in the energy corrections of G_0W_0 with respect to the exact KS eigenvalues (or the HF ones). Considering $\Sigma - V_{xc}^{\mathrm{KS}}$ as a small perturbation, at first order in perturbation theory we get:

$$\epsilon_\pm^{G_0W_0} = \epsilon_\pm^{\mathrm{KS}} + \langle \pm | \, \mathfrak{Re}\left(\hat{\Sigma}(\epsilon_\pm^{G_0W_0}) - \hat{V}_{xc}^{\mathrm{KS}}\right) | \pm \rangle \tag{5.14}$$

where $|\pm\rangle$ are the KS eigenstates (we dropped the σ since these states are spin-independent). This equation is self-consistent in $\epsilon_\pm^{G_0W_0}$, and we can simplify it by linearising with respect to $\epsilon_\pm^{G_0W_0} - \epsilon_\pm^{\mathrm{KS}}$, as done in [9]:

$$\epsilon_\pm^{G_0W_0} = \epsilon_\pm^{\mathrm{KS}} + Z_\pm \langle \pm | \left(\hat{\Sigma}(\epsilon_\pm^{\mathrm{KS}}) - \hat{V}_{xc}^{\mathrm{KS}}\right) | \pm \rangle \qquad \text{with} \qquad Z_\pm = \frac{1}{1 - \frac{\partial \Sigma}{\partial \epsilon}\big|_{\epsilon_\pm^{\mathrm{KS}}}} \tag{5.15}$$

This approach leads to the corrections plotted in Fig. 8, where we see that G_0W_0 gives very good results at low U (though not as good as the HOMO KS solution, which is exact). At higher U and low (or intermediate) values of Δv, G_0W_0 however strongly fails. This means that the G_0W_0 approximation only holds in the low correlation regime, which can be understood in the following way. The real self-energy can be decomposed as $\Sigma = \Sigma_H + \Sigma_x + \Sigma_c$ (in our convention, the Hartree part Σ_H is included in G_0), where Σ_x is the exchange (or Fock) term and $\Sigma_c = \Sigma_c^{\mathrm{screening}} + \Sigma_c^{\mathrm{local}}$. The G_0W_0 approximation gives rise to $\Sigma_{xc}^{G_0W_0} = \Sigma_x + \Sigma_c^{\mathrm{screening}}$, while $\Sigma_c^{\mathrm{local}}$ is contained in the vertex corrections (higher terms in W in Hedin's equations). Thus, when the correlations are weak, electrons delocalise and the screening part of Σ_c is dominant, while on the contrary strong correlations lead to localisation and thus $\Sigma_c^{\mathrm{local}}$ is dominant, explaining the failure of G_0W_0 in this regime.

We can finally note that for $\Delta v = 0$ we indeed find the same energy corrections on Fig. 8 as found by looking at the peaks of the spectral function (see Fig. 7). Despite the failure of G_0W_0 at reproducing the shape of the HOMO and LUMO curves, we can note that it gives a good correction to the fundamental gap $\epsilon_+ - \epsilon_-$ at low Δv, which was widely underestimated by the KS solutions.

5.5 G_0W_0 energy corrections to the restricted Hartree-Fock approximation

Just as we took G^{KS} for the non-interacting G_0 previously, we can as well choose the restricted Hartree-Fock one, G^{RHF}, for the G_0W_0 approximation[6]. Since it is also a non-interacting Green's

[6]Note that G_0 has to be changed both in the expression $\Sigma^{G_0W_0} = iG_0W_0$ and in the calculation of W_0.

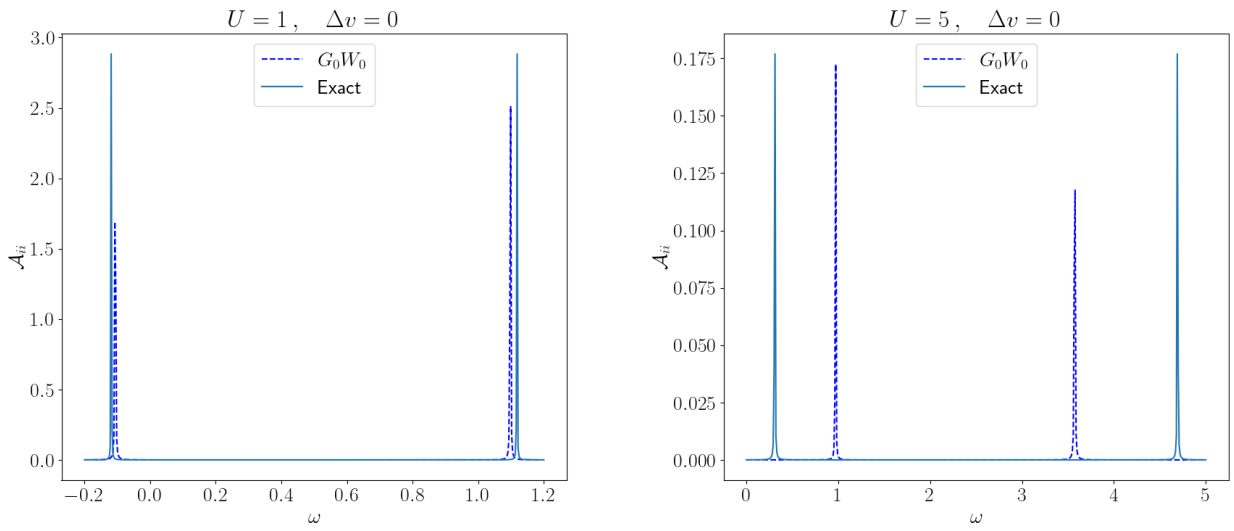

Figure 7: Spectral function of the exact and the G_0W_0 Green's functions with $G_0 = G^{\mathrm{KS}}$, for $U = 1$ and $U = 5$ and $\Delta v = 0$. Only a short range of frequency around the HOMO/LUMO peaks is spanned here.

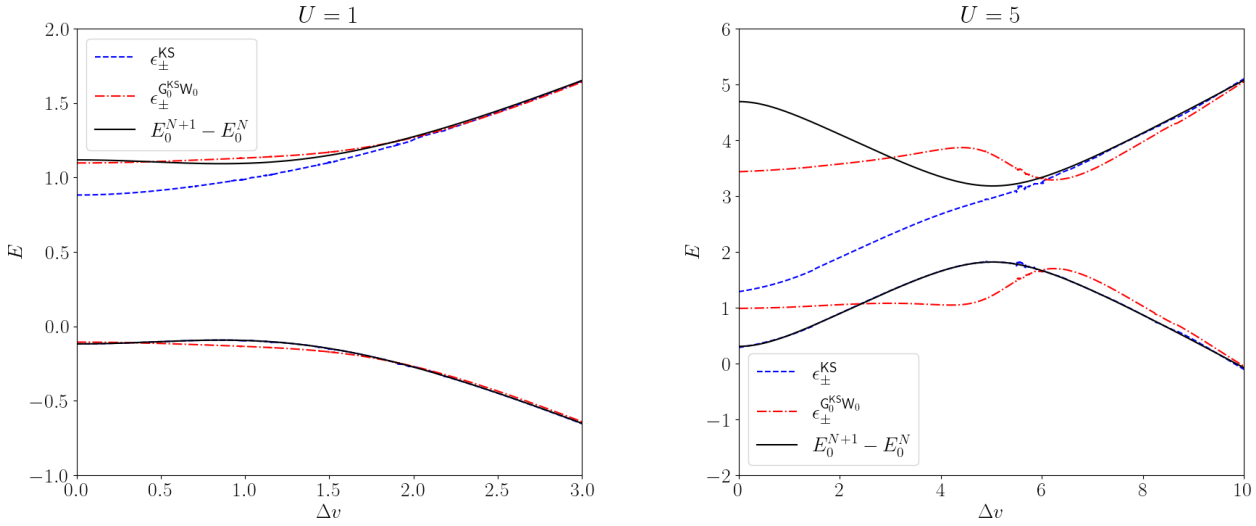

Figure 8: Comparison between the exact energy levels and the HOMO and LUMO G_0W_0 solutions using approximation 5.15 and $G_0 = G^{\mathrm{KS}}$, for $U = 1$ and $U = 5$. The Kohn-Sham solutions are also plotted as a comparison

function, it reads just as the KS one:

$$G^{\mathrm{RHF}}_{ij,\sigma} = \sum_{\pm} \frac{\phi_{\pm\sigma,i}\phi^*_{\pm\sigma,j}}{\omega - \epsilon^{\mathrm{RHF}}_{\pm,\sigma} \pm i0^+} \tag{5.16}$$

and Equations 5.6 still hold, but using ρ^{RHF}, i.e replacing Δv by Δv^{eff} in A.3. Thus, Eq. 5.11 for $\Sigma_{ij}(\omega)$ holds if we replace $\epsilon^{\mathrm{KS}}_{\pm}$ by $\epsilon^{\mathrm{RHF}}_{\pm}$, and ρ^{KS} by ρ^{RHF}.

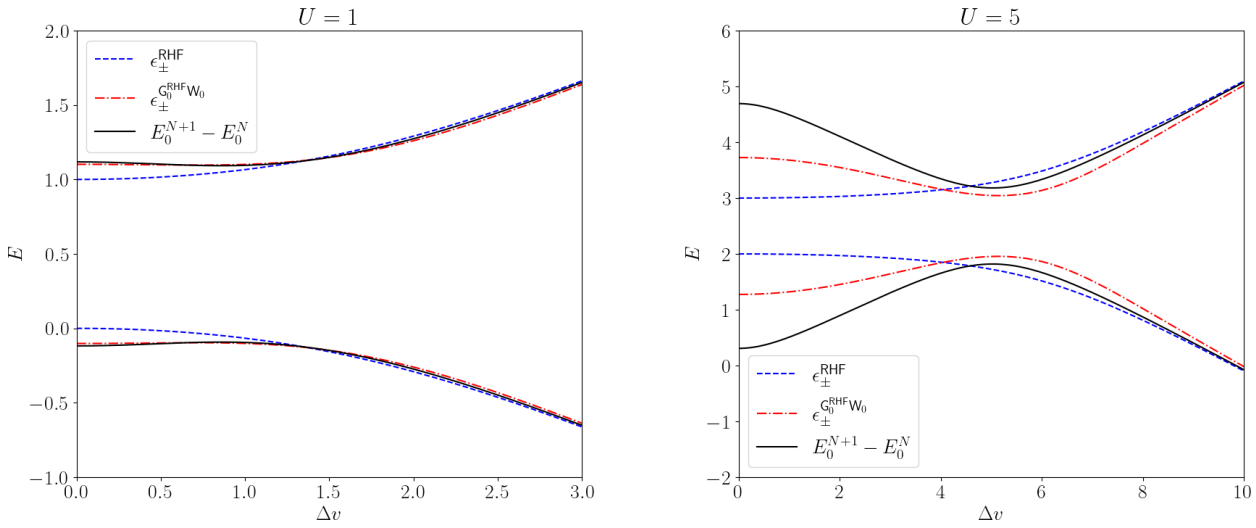

Figure 9: Comparison between the exact energy levels and the HOMO and LUMO G_0W_0 solutions using approximation 5.15 and $G_0 = G^{\mathrm{RHF}}$, for $U = 1$ and $U = 5$. The RHF solutions are also plotted as a comparison

Following the same methods as before[7], we obtain in Fig. 9 the energy corrections from the RHF solutions found in Sec. 4.1. These are globally better than the KS ones, especially for intermediate $\Delta v \sim U$. Even though we expect G^{KS} to be closer to the exact G, there is no reason for $\Sigma^{G_0W_0}$ (which is a truncation of the Hedin development of Σ at first order in W) to be better for G^{KS} than for G^{HF}. Indeed, Σ can be written as an infinite series of G_0 and v_c, whatever the choice of G_0 (as shown in [3]), and this series may converge faster when choosing a simpler G_0, here G^{HF}.

6 Beyond G_0W_0: using the exact screened interaction W

6.1 Exact reducible polarisability

In real materials, G and W are unknown and can only be approximated. Previously, we saw how to compute W_0 within RPA; we could also have computed W^{RPA} using the exact G. In the case of the Hubbard dimer, the exact screened potential W can actually be computed, leading to the G_0W approximation, which becomes semi-exact in the sense that only G is approximate by taking G_0[8]. It is therefore interesting to compare G_0W_0 and G_0W to understand the physics behind these approximations. This has already been done in [3] in the symmetric case, which showed that the exact screened interaction gives a worse result than W_0.

To do so, we compute the reducible polarisability χ (instead of the irreducible one as before), defined by:

$$\chi(1,2) = -i\frac{\delta G(1,1^+)}{\delta U(2)} \tag{6.1}$$

[7]Here instead of subtracting V_{xc}^{KS} from Σ, we rather want to subtract V_x, the exchange potential.

[8]The G_0W approximation is actually, in a sense, beyond GW. Indeed, according to Hedin's equation for $\tilde{\chi}$ (Eq. B.8), the knowledge of the exact W (and thus the exact $\tilde{\chi}$) involves the knowledge of the exact vertex $\tilde{\Gamma}$.

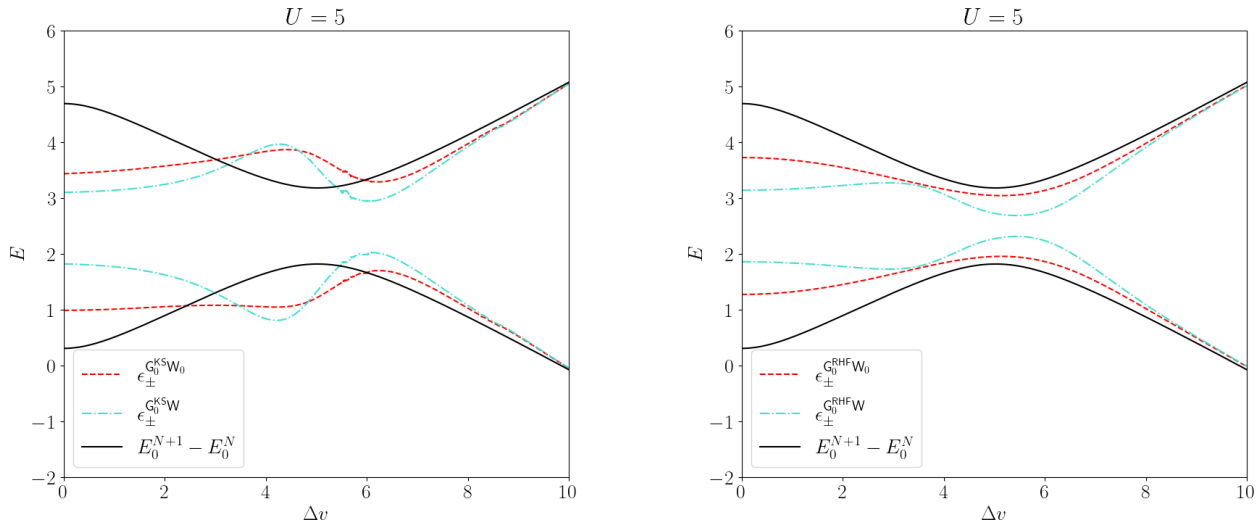

(a) $G_0 = G^{\mathrm{KS}}$ (b) $G_0 = G^{\mathrm{RHF}}$

Figure 10: Comparison between the exact energy levels and the HOMO and LUMO G_0W solutions using approximation 5.15, the self-energy given by Eq. 6.8 and $G_0 = G^{\mathrm{KS}}$ or G^{RHF}, for $U = 5$. The respective G_0W_0 solutions are also plotted as a comparison

which is simply the variation of the electronic density with respect to an external field. Moreover, thanks to the relation B.3, we can express χ in terms of the 1-GF and the 2-GF:

$$\chi(1,2) = iG_2(1,2;1^+,2^+) - iG(1,1^+)G(2,2^+) \tag{6.2}$$

where the 2-GF is the two-particle Green's function, defined as:

$$G^{(2)}(1,2;3,4) = -\left\langle \hat{T}\left[\hat{\psi}(1)\hat{\psi}(2)\hat{\psi}^\dagger(4)\hat{\psi}^\dagger(3)\right]\right\rangle \tag{6.3}$$

which, just as the 1-GF, has a simple form in the Lehmann representation. W is then given in terms of χ by:

$$W(1,2) = v_c(1,2) + \int \mathrm{d}3\ \mathrm{d}4\ v_c(1,3)\chi(3,4)v_c(4,2) \tag{6.4}$$

6.2 G_0W in the case of the asymmetric Hubbard dimer at half-filling

In the case of the Hubbard dimer, we find that χ reads, in the site-basis and in frequency space:

$$\chi_{ij\sigma\sigma'}(\omega) = \sum_{n=2,3,4} \alpha^{(n)}_{ij\sigma\sigma'}\left[\frac{1}{\omega - (E_n - E_1) + i0^+} - \frac{1}{\omega + (E_n - E_1) - i0^+}\right] \tag{6.5}$$

where the sum runs over the excited states of the $N = 2$ system, the $\alpha^{(n)}_{ij\sigma\sigma'}$ are coefficients that we can compute using the $N = 2$ eigenstates (see Appendix A):

$$\alpha^{(n)}_{ij\sigma\sigma'} = \langle 1|\, \hat{c}^\dagger_{i\sigma}\hat{c}_{i\sigma}\,|n\rangle\,\langle n|\, \hat{c}^\dagger_{j\sigma'}\hat{c}_{j\sigma'}\,|1\rangle \tag{6.6}$$

and the exact screened potential W reads:

$$W_{ij}(\omega) = U\delta_{ij} + U^2 \sum_{\sigma\sigma'} \chi_{ij\sigma\sigma'} \tag{6.7}$$

Contrary to what is found in [3], we don't find $W_{11} = W_{22}$. This was expected due to the asymmetry of the two sites. We still find however that $W_{12} = W_{21}$. Finally, Eq. 5.3 enables us to compute the self-energy within the G_0W approximation, and we find after integration in the complex plane:

$$\Sigma_{ij}^{G_0W}(\omega) = -\frac{Un_i}{2}\delta_{ij} + 4U^2 \sum_{n=3,4} \beta_i^{(n)}\beta_j^{(n)} \left[\frac{\phi_{+,i}\phi_{+,j}}{\omega - (E_n - E_1 + \epsilon_+) + i0^+} + \frac{\phi_{-,i}\phi_{-,j}}{\omega + (E_n - E_1 - \epsilon_-) - i0^+} \right] \tag{6.8}$$

where $\phi_{\pm,i}$ is defined by Eq. 5.6, $\epsilon_\pm$ are the KS (or RHF) eigenenergies, and the coefficients β_i are defined by:

$$\beta_1^{(n)} = \frac{\left(a_1 - \frac{E_1}{t}\right)\left(a_n - \frac{E_n}{t}\right)}{\mathcal{N}_1\mathcal{N}_n} \qquad \beta_2^{(n)} = \frac{1 + a_1a_n}{\mathcal{N}_1\mathcal{N}_n} \tag{6.9}$$

with $a_n = \frac{2t}{E_n - \Delta v - U}$ and $\mathcal{N}_n$ the normalisation factor of the $N = 2$ eigenstates. Comparing Eq. 6.8 with Eq. 5.11, it is striking that Σ has the same structure in both the G_0W_0 and the G_0W approximations.

The linearised solutions at first order in perturbation theory (given by Eq. 5.15) are plotted in Fig. 10a for $G_0 = G^{\mathrm{KS}}$, and in Fig. 10b for $G_0 = G^{\mathrm{RHF}}$. As we can see with the naked eye, the G_0W results are worse than the G_0W_0 ones, which is counter-intuitive. This is a generalisation of the same observation made in [3] for $\Delta v = 0$. It is thus preferable to be consistent in our approximation (i.e choosing a non-interacting G_0 everywhere) than only approximating G_0 in Σ but using the exact G for computing W. This can be interpreted as follows. When fully taking into account the vertex corrections (both in the expression of Σ and in W), some terms cancel out, which is not the case when we only correct W while taking $\Sigma = iG_0W$. In other words, a consistent choice of G_0 everywhere leads to error cancelling and thus gives a better result.

7 Discussion of the band offset in the Hubbard dimer

It is finally interesting to make the link between the Hubbard dimer model and real materials. When dealing with heterostructures, an important quantity is the band offset, generally the valence one, defined by the shift of the valence bands of the two materials at the junction. In our case, instead of bands we only have two energies: the levels $E^{N\pm1} - E^N$ associated to the addition/removal of one electron, and it is not trivial to say that each of them is associated to one site, since the ground states for $N = 1, 2, 3$ are not totally localised, except in the limit $\Delta v \to +\infty$.

In other words, what we want to define a band offset are energy bands (which are local quantities), while what is measured and computed here are many-body addition/removal energies (or levels), which are global.

We can however take advantage of the analysis of the restricted Hartree-Fock approximation (see Sec. 4.1), since according to Koopman's theorem, the RHF eigenenergies $\epsilon_\pm^{\mathrm{RHF}}$ can be in-

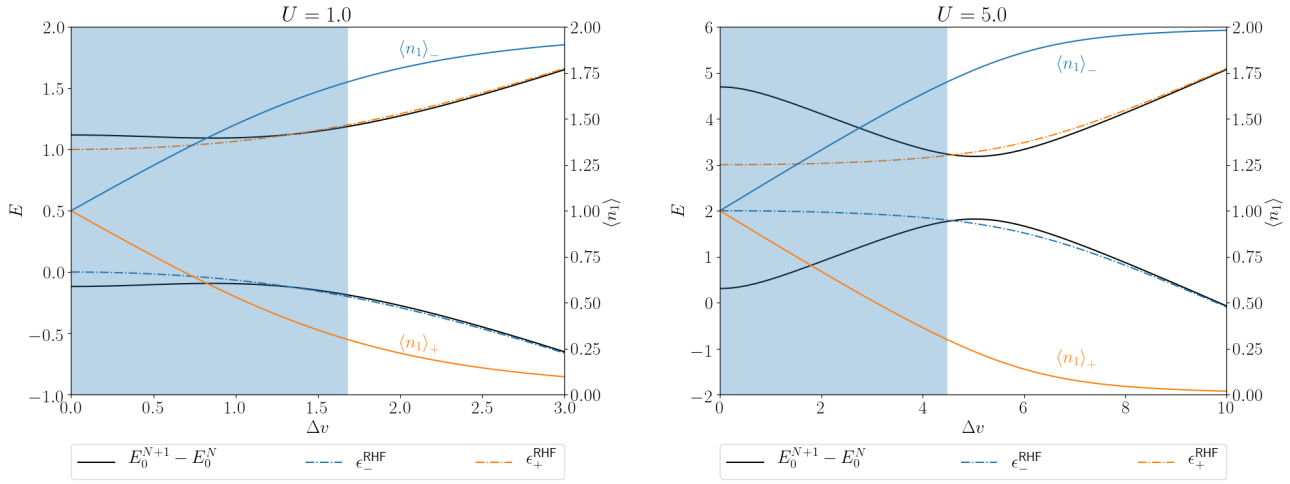

Figure 11: RHF occupation number $\langle \hat{n}_1 \rangle$ for both $|\pm\rangle$ eigenstates as well as the RHF eigenenergies $\epsilon_\pm^{\text{RH}}$ (in dash-dotted lines) and the exact energy levels (in solid black lines). The white area is the Δv domain for which $\langle \hat{n}_1 \rangle_- = \langle \hat{n}_2 \rangle_+ > \alpha$, with here $\alpha = 1.7$.

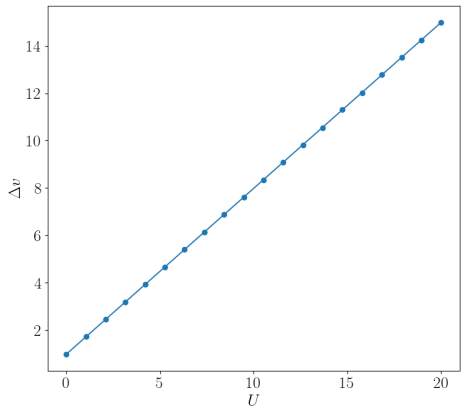

Figure 12: Critical value of Δv for the localisation criterion (with $\alpha = 1.7$), with respect to U.

terpreted as addition/removal energies. We know from our analysis that RHF solutions give reasonable energy levels for $\Delta v \gtrsim U$. The RHF eigenstates and occupation number are given by Eq. 4.6, from which we can already see that the electrons tend to localise with increasing Δv. We can choose as an arbitrary criterion that when $\langle \hat{n}_1 \rangle_- = \langle \hat{n}_2 \rangle_+$ is greater than some value α, the RHF $|\pm\rangle$ states (and consequently the energies $\epsilon_\pm^{\text{RH}}$) can be assigned to sites 1 and 2 respectively. In Fig. 11, we plotted the occupation number $\langle \hat{n}_1 \rangle_\pm$ on top of the RHF eigenenergies and the exact energy levels. As we can see, choosing $\alpha = 1.7$ (which is not a very restrictive criterion), the values of Δv for which the states are localised (the white area on the graph) match with the ones for which the RHF approximation is good.

We can estimate roughly that the transition from delocalised RHF states (blue area) to localised ones occurs at $\Delta v_{\text{critical}} \sim U$. This is very well verified in Fig. 12. In photovoltaic materials (such as silicon or perovskites), the correlations are often small, meaning that $\Delta v \gtrsim U$, in which case we can define the band offset as $\epsilon_+^{\text{RH}} - \epsilon_-^{\text{RH}}$, i.e as the band gap of our system within the RHF approximation.

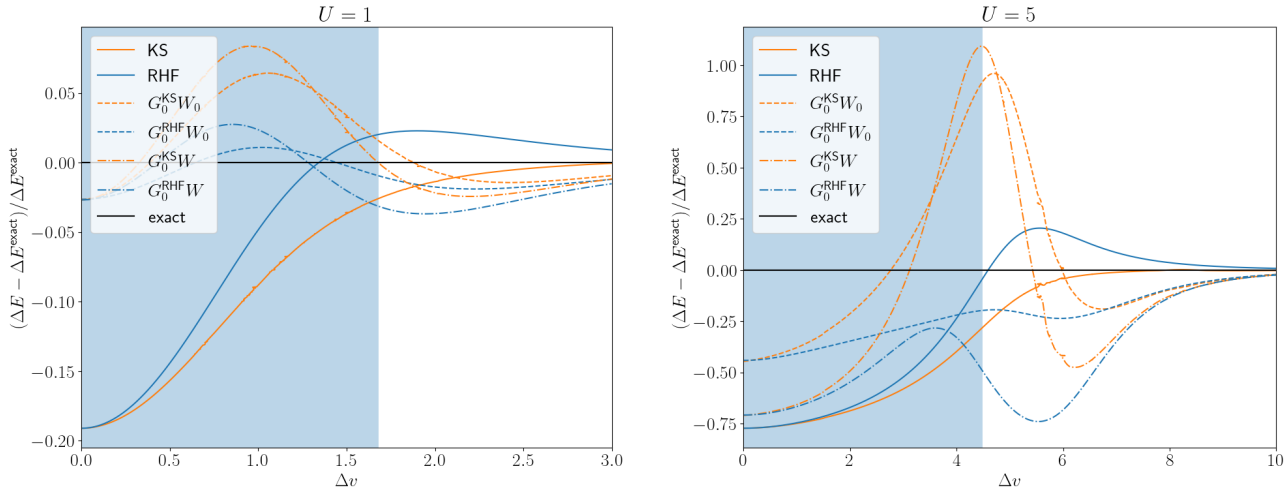

Figure 13: Band gaps within the exact KS framework and the RHF and GW approximations, relatively to the exact band gap $2E^{N=2} - E^{N=1} - E^{N=3}$. The KS-related schemes are presented in orange, while the HF-related ones are in blue.

As a summary, we can compare the band gaps obtained with exact KS, RHF and the four different flavours of GW for $\Delta v > \Delta v_{\mathrm{critical}}$, i.e in the region where the band gap can be understood as a band offset. In Fig. 13, we can see that the exact KS gap is slightly underestimated, while the RHF one is slightly overestimated. The G_0W_0 gaps are worse, and only barely better than the G_0W ones.

8 Conclusion

The Hubbard dimer is a toy model, supposed to describe the neighborhood of the junction in a heterostructure. It is of course far from realistic materials but has the advantage of being exactly solvable, which makes it a good benchmark for comparing different approximations. In this thesis, we explored the exact Kohn-Sham solutions and the (restricted and unrestricted) Hartree-Fock approximation, which are the two main approaches in which electronic interactions are replaced by effective potentials in a non-interacting system. Many-body effects are only partially captured in these schemes when correlations become too strong, even though they constitute a very good starting point - especially the unrestricted HF approximation, which allows for anti-ferromagnetic solutions, a specificity of the Hubbard dimer. In order to go further independent-particle approaches, we then implemented the G_0W_0 approximation, a fundamentally many-body-oriented and very popular tool for computing band offsets in real systems. This analysis was performed for both KS and HF Green's functions, which are non-interacting. It appeared that G_0W_0 energy levels are worse than the respective non-interacting methods, except in the symmetric limit. At first sight, a refinement of G_0W_0 (which is beyond GW in a sense) is to compute the exact screened potential W and proceed to a G_0W approximation. But despite this apparent enhancement, G_0W energy levels proved to be even worse than G_0W_0 ones, giving interesting insights about the way these approximations work. Finally, we used our knowledge of the Hubbard dimer to discuss the band offset problem, clarifying the bridge between our two-site-model and a real heterostructure.

When computing Σ^{G_0W}, we only took into account vertex corrections in W, but we still took $\tilde{\Gamma} = 1$ in $\Sigma = iGW\tilde{\Gamma}$. A next interesting step in order to go beyond GW and better correct the energy levels at high correlations would be to include vertex corrections in both Σ and W. This is however much more difficult to achieve.

Another interesting perspective would be to improve the model into a more realistic one. For instance, we could extend the dimer into two semi-infinite chains. Alternatively, we could keep the two sites but consider a two-orbital model.

9 Bibliography

[1] E. Khorani, C. A. Messmer, S. L. Pain, T. Niewelt, B. F. M. Healy, A. Wratten, M. Walker, N. E. Grant, and J. D. Murphy, "Electronic band offset determination of oxides grown by atomic layer deposition on silicon," *IEEE Journal of Photovoltaics*, 2023.

[2] A. Lorin, T. Bischoff, A. Tal, and A. Pasquarello, "Band alignments through quasiparticle self-consistent GW with efficient vertex corrections," *Phys. Rev. B*, Dec 2023.

[3] A. El Sahili, "Des spectres à l'énergie totale : au-delà de l'approximation GW pour concevoir des interactions effectives." Ph.D. dissertation, 2024, directed by Lucia Reining and Francesco Sottile, Institut polytechnique de Paris.

[4] M. Vanzini, "Dynamical local connector approximation for electron addition and removal spectra," 2017.

[5] P. Hohenberg and W. Kohn, "Inhomogeneous electron gas," *Phys. Rev.*, vol. 136, Nov 1964.

[6] W. Kohn and L. J. Sham, "Self-consistent equations including exchange and correlation effects," *Phys. Rev.*, vol. 140, Nov 1965.

[7] K. Schönhammer, O. Gunnarsson, and R. M. Noack, "Density-functional theory on a lattice: Comparison with exact numerical results for a model with strongly correlated electrons," *Phys. Rev. B*, vol. 52, Jul 1995.

[8] D. J. Carrascal, J. Ferrer, J. C. Smith, and K. Burke, "The Hubbard dimer: a density functional case study of a many-body problem," *Journal of Physics: Condensed Matter*, sep 2015.

[9] F. Bruneval, "Exchange and correlation in the electronic structure of solids, from silicon to cuprous oxide: GW approximation and beyond," Master's thesis, Ecole Polytechnique, 2005.

[10] R. M. Martin, L. Reining, and D. M. Ceperley, *Interacting Electrons: Theory and Computational Approaches*. Cambridge University Press, 2016.

[11] L. Hedin, "New method for calculating the one-particle green's function with application to the electron-gas problem," *Phys. Rev.*, vol. 139, Aug 1965.

A Exact eigenstates

A.1 $N = 1$

In the basis $(|\uparrow, 0\rangle, |\downarrow, 0\rangle, |0, \uparrow\rangle, |0, \downarrow\rangle)$,

$$H^{N=1} = \begin{pmatrix} v_1 & 0 & -t & 0 \\ 0 & v_1 & 0 & -t \\ -t & 0 & v_2 & 0 \\ 0 & -t & 0 & v_2 \end{pmatrix} \tag{A.1}$$

Diagonalising this Hamiltonian gives two spin-degenerate eigenstates:

$$\begin{aligned} |+, \sigma\rangle &= \sin\rho\, |\sigma, 0\rangle - \cos\rho\, |0, \sigma\rangle \\ |-, \sigma\rangle &= \cos\rho\, |\sigma, 0\rangle + \sin\rho\, |0, \sigma\rangle \end{aligned} \tag{A.2}$$

with ρ defined by:

$$\tan\rho = -\frac{\Delta v}{2} + \sqrt{1 + \frac{\Delta v^2}{4}} \tag{A.3}$$

A very useful result is the occupation difference for $N = 1$, given by:

$$\Delta n = n_1 - n_2 = \frac{2\Delta v}{\sqrt{4t^2 + \Delta v}} \tag{A.4}$$

A.2 $N = 2$

In the basis $(|\uparrow\downarrow, 0\rangle, |\uparrow, \downarrow\rangle, |\downarrow, \uparrow\rangle, |0, \uparrow\downarrow\rangle)$,

$$H^{N=2} = \begin{pmatrix} 2v_1 + U & -t & t & 0 \\ -t & v_1 + v_2 & 0 & t \\ t & 0 & v_1 + v_2 & -t \\ 0 & t & -t & 2v_2 + U \end{pmatrix} \tag{A.5}$$

We find 4 non-degenerate eigenstates:

$$|\lambda\rangle = \begin{cases} \frac{1}{\mathcal{N}_\lambda}\left[(|\uparrow, \downarrow\rangle - |\downarrow, \uparrow\rangle) + \frac{2}{E_\lambda - \Delta v - U}\left(|\uparrow\downarrow, 0\rangle - |0, \uparrow\downarrow\rangle\right) - E_\lambda\, |\uparrow\downarrow, 0\rangle\right] & \text{for } \lambda \neq 2 \\ \frac{1}{\sqrt{2}}\left(|\uparrow, \downarrow\rangle - |\downarrow, \uparrow\rangle\right) & \text{for } \lambda = 2 \end{cases} \tag{A.6}$$

with $\mathcal{N}_\lambda$ a proper normalisation factor.

A.3 $N = 3$

In the basis $(|\uparrow\downarrow,\uparrow\rangle, |\uparrow\downarrow,\downarrow\rangle, |\uparrow,\uparrow\downarrow\rangle, |\downarrow,\uparrow\downarrow\rangle)$,

$$H^{N=3} = \begin{pmatrix} 2v_1 + v_2 + U & 0 & -t & 0 \\ 0 & 2v_1 + v_2 + U & 0 & -t \\ -t & 0 & 2v_2 + v_1 + U & 0 \\ 0 & -t & 0 & 2v_2 + v_1 + U \end{pmatrix} \tag{A.7}$$

This Hamiltonian is the same as $H^{N=1}$ provided we redefine on-site energies:

$$\begin{cases} v_1' = 2v_1 + v_2 + U = v_1 + U \\ v_2' = 2v_2 + v_1 + U = v_2 + U \end{cases} \tag{A.8}$$

Since $\Delta v' = \Delta v$, the eigenstates are the same as for $N = 1$ according to Eq. A.3.

B Functional derivative formalism and Hedin's equations

In order to go beyond the single-electron picture, and in particular HF, we have to write the equation of motion of the one-particle Green's function in terms of the two-particle one [9, 10]:

$$\left[i\frac{\partial}{\partial t_1} - h(\mathbf{r}_1) \right] G(1,2) + i \int \mathrm{d}3\, v_c(1,3) G_2(1,3^+;2,3^{++}) = \delta(1,2) \tag{B.1}$$

Where the notation $G(1,2)$ refers to $G(\mathbf{r_1}, t_1, \sigma_1; \mathbf{r_2}, t_2, \sigma_2)$, and where (1^+) means $(\mathbf{r_1}, t_1^+, \sigma_1)$[9]. The second term of the left hand side of Eq. B.1 defines the self-energy:

$$\int \mathrm{d}3\, \Sigma(1,3) G(3,2) = -i \int \mathrm{d}3\, v_c(1,3) G_2(1,3^+;2,3^{++}) \tag{B.2}$$

Eq. B.1 is useless as it is since we don't know the two-particle Green's function G_2 (in order to compute it, we would need the three-particle one, and so on). However, G_2 can be expressed as a functional derivative of G with respect to an external infinitesimal potential U:

$$\frac{\delta G(1,2)}{\delta U(3,4)} = -G_2(1,4;2,3) + G(1,2)G(4,3) \tag{B.3}$$

Following Hedin's idea [11], as explained in [9], we want to perform perturbation theory with respect to the screened Coulomb potential W rather than on the bare one. We start by including the Hartree potential in U by defining:

$$V(1) = U(1,1) - i \int \mathrm{d}2\, v_c(1,2) G(2,2^+) \tag{B.4}$$

[9] where $t^+ = t + i\eta$ with $\eta \to 0$

and we find that the self-energy reads:

$$\boxed{\Sigma(1,2) = i \int \mathrm{d}3\,\mathrm{d}4\, G(1,4) W(3,1^+) \tilde{\Gamma}(4,2;3)} \tag{B.5}$$

where the irreducible[10] vertex function $\tilde{\Gamma}$ is defined by:

$$\tilde{\Gamma}(1,2;3) = \delta(1,2)\delta(1,3) + \frac{\delta\Sigma(1,2)}{\delta V(3)} \tag{B.6}$$

and the screened Coulomb potential is:

$$W(1,2) = v(1,2) + \int \mathrm{d}3\,\mathrm{d}4\, v(1,3)\tilde{\chi}(3,4)W(4,2) \tag{B.7}$$

$\tilde{\chi}$ is the irreducible polarisability, and can be expressed either in terms of the inverse dielectric function, or directly by:

$$\tilde{\chi}(1,2) = -i\frac{\delta G(1,1^+)}{\delta V(2)} = -i \int \mathrm{d}3\,\mathrm{d}4\, G(2,3)G(4,2)\tilde{\Gamma}(3,4;1) \tag{B.8}$$

Thanks to this complete set of equations (called Hedin's equations), we are now theoretically able to find Σ and thus G, by self-consistent iterations for instance. However this process is excessively costly in practice, and good approximations are thus needed to reduce the complexity.

[10] Here and in the rest of the report, irreducible means that functional derivatives are performed with respect to V instead of U